The Cytoskeleton of the Resting Human Blood Platelet: Structure of the Membrane Skeleton and Its Attachment to Actin Filaments

John H. Hartwig*‡ and Michelle DeSisto*

*Hematology-Oncology Unit, Department of Medicine, and the ‡Department of Anatomy and Cellular Biology, *Massachusetts General Hospital and *‡Harvard Medical School, Charlestown, Massachusetts 02129

Abstract. We used high-resolution EM and immunocytochemistry in combination with different specimen preparation techniques to resolve the ultrastructure of the resting platelet cytoskeleton. The periphery of the cytoskeleton, an electron-dense subplasmalemmal region in thin section electron micrographs, is a tightly woven planar sheet composed of a spectrin-rich network whose interstices contain GPIb/IX-actin-binding protein (ABP) complexes. This membrane skeleton connects to a system of curved actin filaments (F-actin) that emanate from a central oval core of F-actin cross-linked by ABP. The predominant interaction of the radial actin filaments with the membrane skeleton is along their sides, and the strongest connection between the membrane skeleton and F-actin is via ABP-GPIb ligands, although there is evidence for spectrin attaching to the ends of the radial actin filaments as well. Since a mechanical separation of the F-actin cores and radial F-actin-GPIb-ABP complexes from the underlying spectrin-rich skeleton leads to the latter's expansion, it follows that the spectrin-based skeleton of the resting cell may be held in a compressed form by interdigitating GPIb/IX complexes which are immobilized by radial F-actin-ABP anchors.

THE human blood platelet is an interesting and versatile cell. After release from the periphery of a megakaryocyte in the bone marrow, it circulates as a disc known conventionally as the resting platelet. In this state it must passively resist high arterial pressures that buffet it against vessel walls. Then, when it encounters hemostatic agonists such as thrombin and ADP, it undergoes an active series of radical shape alterations beginning with the extension of veils and filopodia. This transformation generates a plastic structure ideally suited to seal leaks in the vasculature and to engage fibrin strands formed by the blood coagulation cascade. Subsequently, the platelet acquires yet another role, becoming a contractile motor for retraction of fibrin, thereby increasing the tension within the fibrin clot and strengthening it.

Actin is the major platelet protein and ~40% of it is in the form of filaments (F-actin) in the resting cell. During platelet activation the level of cytoplasmic F-actin increases markedly and this newly assembled actin fills the projections extended by the cell (16, 20, 21, 40). Some actin modulating proteins such as profilin, gelsolin, and a small polypeptide called Fx, control linear actin assembly in response to platelet activating stimuli (10, 11, 13, 14, 29), while others such as actin-binding protein (ABP)[1] establish the three-dimensional architecture of the assembled filaments (9, 36).

This paper reports new findings regarding the structure of the resting platelet cytoskeleton. It has long been known that in addition to F-actin, resting platelets contain microtubules that coil around the cell periphery immediately beneath and parallel to the plasma membrane. Fox (3) and Okita et al. (25) independently discovered that some of the F-actin in resting platelets is associated with the plasma membrane through the intermediary of ABP, which binds both F-actin and the transmembrane glycoprotein Ib/IX complex. Boyles (1, 5) and others (23), in addition, have provided ultrastructural evidence that delipidated platelets have an electron-dense structure that invests the cell periphery, implying the existence of a submembrane lamina analogous to the well-defined spectrin-rich shell of the erythrocyte. We have used detergent-permeabilization followed by rapid-freezing, freeze-drying, and metal shadowing to obtain high resolution images of cytoskeleton of the resting platelet. This approach has provided sharply defined views of the membrane skeleton and has demonstrated its substructure and how it connects with cytoplasmic actin filaments. Immunoelectron microscopy was used to demonstrate that the resting membrane skeleton is composed of two fundamental systems: GPIb/IX complexes connected to underlying F-actin by ABP molecules and a spectrin-containing meshwork. Actin filaments emerge in a radial fashion from a core of actin filaments cross-linked by ABP to associate with the membrane skeleton on their sides and ends but long actin filaments do not appear to be an integral component of the spectrin-based meshwork.

1. *Abbreviations used in this paper*: ABP, actin-binding protein.

Materials and Methods

Preparation of Cells

Platelets. Anticoagulated normal human blood was centrifuged at 110 *g* for 10 min and the platelet-rich plasma was gel-filtered through a Sepharose 2B column equilibrated and eluted with a buffer containing 145 mM NaCl, 10

mM Hepes, 10 mM glucose, 0.5 mM Na_2HPO_4, 5 mM KCl, 2 mM $MgCl_2$, and 0.3% BSA, pH 7.4. Platelets were used only after a 60-min incubation at 37°C as previously reported (10, 11).

Electron Microscopy

Embedding and Sectioning of Platelet Cytoskeletons. Resting platelets were permeabilized by the addition of one-tenth volume of 0.6 M Pipes, 0.25 M Hepes, 0.1 M EGTA, 20 mM $MgCl_2$ (10× PHEM buffer of Schliwa et al. [30]), 7.5% Triton X-100 and 10% glutaraldehyde. After 15 min the cytoskeletons were pelleted, and the pellet dehydrated and embedded in Lowicryl K4M as previously described (10).

Rapid-Freezing and Freeze-Drying. Replicas of intact cytoskeletons were prepared by adding one-tenth volume of 10× PHEM-Triton buffer containing 10% glutaraldehyde and 50 μM phallacidin to suspended cells and allowing permeabilization to proceed for 10 min. The resultant cytoskeletons were allowed to adhere to the surface of a polylysine-coated coverslip, the coverslip extensively washed with distilled water, rapidly frozen, freeze-dried, and rotary coated with metal and carbon. This approach yielded intact cytoskeletons, whose dense metal coats did not allow for visualization of the cytoskeleton's interior. In experiments designed to separate the membrane skeleton from its underlying core, detergent permeabilization of cells was done with one-tenth volume of 10× PHEM-Triton for 2 min in the absence or presence of a final concentration of 0.1% glutaraldehyde and 5 μM phallacidin or 0.1% glutaraldehyde alone, depending on the desired openness of the resultant membrane skeleton. The resulting cytoskeletons were made 1% with glutaraldehyde for 10 min then adhered to freshly glow-discharged glass coverslips (5-mm-diam, round) by centrifugation. Solutions of 250 μl of platelet cytoskeletons in suspension were placed in wells of a 96-well microtiter plate each containing a coverslip and the plate centrifuged at 1,460 *g* for 5 min at 25°C. Adherent cytoskeletons from cells were then washed into distilled water and rapidly-frozen. As discussed in Results, cytoskeletons treated in this fashion rupture during the centrifugation process, separating sheets of membrane skeleton from more three-dimensional cytoskeletal cores.

Labeling with Myosin S1. Fixed, glass adherent cytoskeletons were incubated with 25 μl of 2 mg/ml rabbit skeletal myosin subfragment 1 for 5 min, washed thrice in 0.15 M NaCl, 10 mM sodium phosphate buffer, pH 7.4 (PBS), and fixed in 1% glutaraldehyde, 0.2% tannic acid, and 10 mM sodium phosphate buffer, pH 7.0.

Treatment of Cytoskeletons with Buffers Containing Calcium and Plasma Gelsolin or ATP. Resting cells were permeabilized for 2 min either with Triton-PHEM or with Triton-PHCM buffer containing 1 mM $CaCl_2$ instead of 10 mM EGTA, and in either case 4.2 nM leupeptin, 1 mM benzamidine, and 12.3 nM aprotinin (protease inhibitors) in the absence of added fixatives for 1 min. The cells were then centrifuged onto glass coverslips. Control (EGTA-permeabilized) and calcium-permeabilized cytoskeletons were then fixed with 1% glutaraldehyde for 10 min. Unfixed EGTA-permeabilized cytoskeletons were treated either with (*a*) affinity purified human plasma gelsolin at concentrations of 10, 25, 50, and 100 μg/ml (41) in the presence of 1 mM $CaCl_2$ for 2 min at 25°C, or (*b*) PHEM containing 10 mM ATP for 10 min. Both gelsolin-treated and PHEM-treated cytoskeletons were fixed with 1% glutaraldehyde-PHEM for 10 min, followed by rapid freezing.

Labeling of Platelet Sections and Cytoskeleton with Antibodies and Anti-Primary Antibody-Coated Gold Particles. 5-15-nm-diam colloidal gold particles were prepared with tannic acid (34) and coated with affinity-purified rabbit anti-goat IgG, goat anti-mouse IgG, or goat anti-rabbit IgG all which had been absorbed with human IgG. Polyclonal affinity-purified goat anti-rabbit macrophage myosin IgG was used in all immunohistochemical studies. Its preparation has been previously described (33, 35). A mouse anti-human GPIb mAb was generously supplied by Dr. Burt Adelman (Medical College of Virginia, Richmond, VA) and has been characterized by us in a previous study (2). The affinity-purified goat anti-rabbit macrophage ABP IgG has been characterized in a number of previous studies (9, 10, 11). Affinity purified rabbit anti-human brain fodrin (nonerythroid spectrin) antibodies were provided by Dr. Jon Morrow (Yale Medical School, New Haven, CT) and anti-sea urchin egg spectrin antibodies were provided by Dr. David Begg (Harvard Medical School, Boston, MA). The platelet specificity of the anti-brain spectrin antibody was reported in (6). To label the cell sections with gold, cut sections were placed on the surface of 10-μl drops of 10 μg/ml of mouse monoclonal or affinity-purified goat antibody in PBS containing 1% BSA, pH 8.2 (PBS-BSA) and incubated for 1 h at 25°C. Sections were washed thrice by transferring them to drops of PBS/BSA for 5 min each. They were then transferred to 10-μl drops of PBS-BSA containing anti-primary IgG-coated gold. After the incubation with IgG-gold, the sections were washed twice in PBS, thrice in distilled water and stained with 2% uranyl acetate for 7 min followed by lead citrate for 1 min. Sections were viewed and photographed in a JEOL 1200-EX electron microscope at an accelerating voltage of 80 kV. To label glass adherent cytoskeletons, residual fixative was blocked with 0.1% sodium borohydride in PHEM buffer, and cells were washed twice in PBS and twice in PBS containing 1% BSA, pH 8.2. Coverslips were covered with 25 μl of primary antibodies at a concentration of 10 μl/ml, incubated for 1 h at 25°C, and washed thrice with PBS/BSA. Coverslips were then incubated for 1.5 h with the appropriate IgG-colloidal gold particles (1:10 dilution of rabbit anti-gold IgG and 1:20 dilutions of goat anti-mouse IgG and goat anti-rabbit IgG), washed thrice in PBS/BSA, thrice in PBS, and fixed with 1% glutaraldehyde in 10 mM sodium phosphate buffer for 10 min. Fixed specimens were washed extensively with distilled water, rapidly-frozen and freeze-dried, and rotary coated with platinum or tantalum-tungsten at 45° and carbon at 90° as previously described.

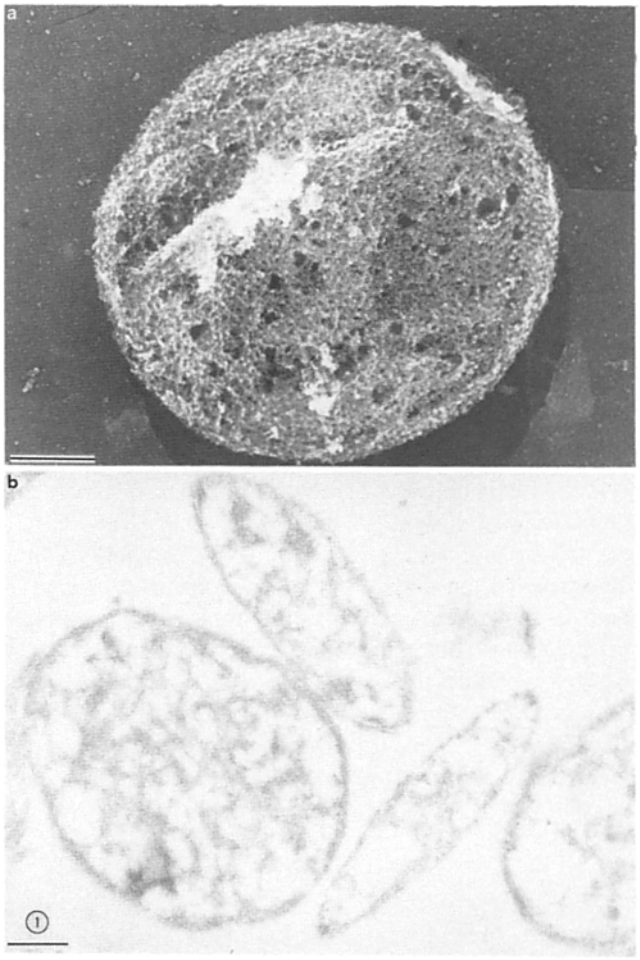

Figure 1. Structure of the intact platelet cytoskeleton prepared by fixing cells with 1% glutaraldehyde during permeabilization. Platelets were permeabilized with PHEM-Triton containing 1% glutaraldehyde. Cells were adhered to polylysine-coated coverslips and washed with PHEM buffer. (*a*) Replica of intact resting cytoskeleton. (*b*) Thin section through Epon-embedded cytoskeletons. Bars, 0.5 μm.

SDS-PAGE. Resting cells were extracted with 0.75% Triton X-100 in PHEM buffer containing the above mentioned protease inhibitors. Samples of the total platelet lysate were taken for total protein analysis and for SDS-PAGE by the addition of one-tenth volume of 2% SDS, 20 mM β-mercaptoethanol, 250 mM Tris, 50% glycerol, pH 6.8 followed immediately by boiling for 5 min. After 2 min, resultant cytoskeletons were pelleted by centrifugation at 100,000 *g* for 15 min in a ultramicrocentrifuge (TL-100;

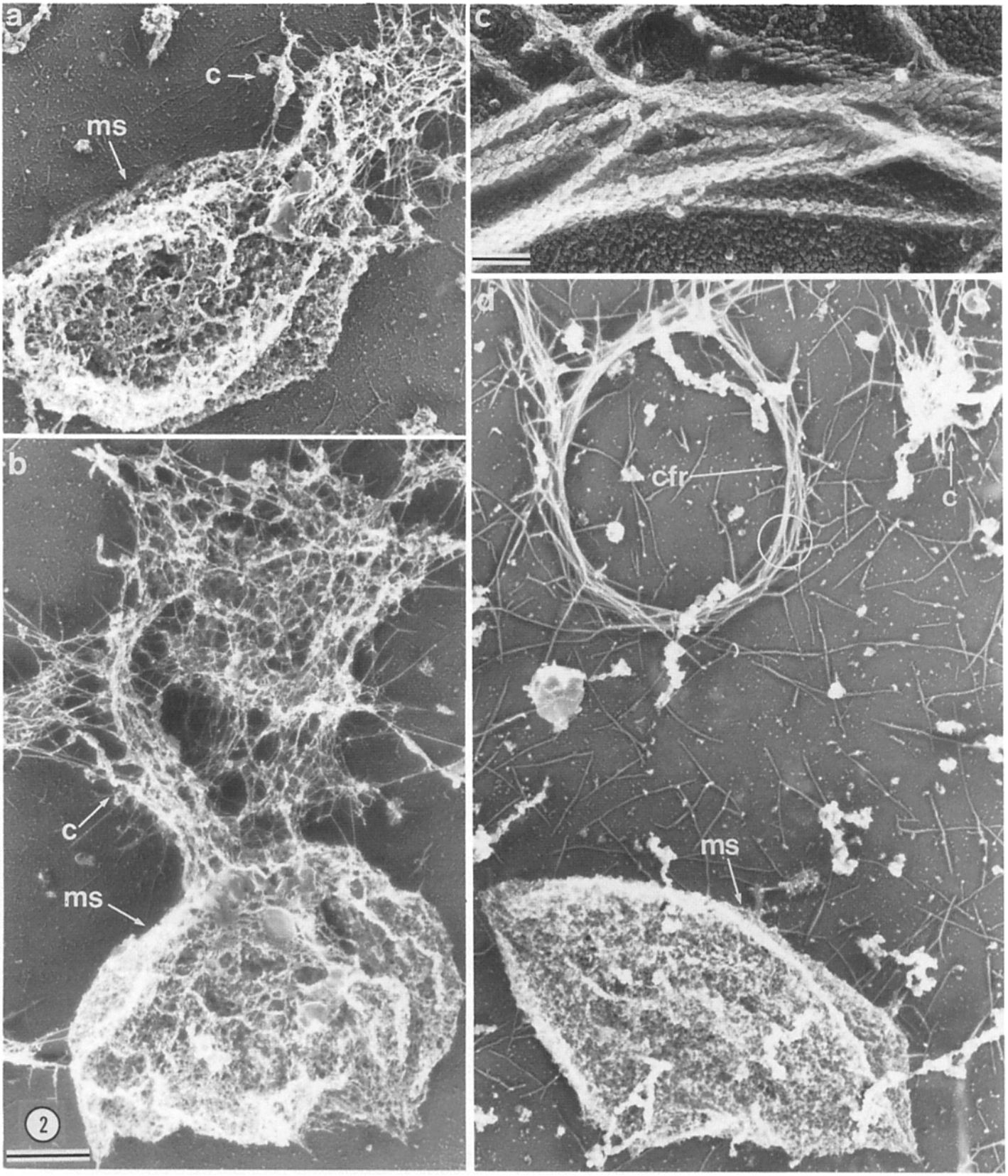

Figure 2. Gallery of representative low-magnification electron micrographs of the detergent insoluble platelet cytoskeletal components as pelleted onto the surface of a coverslip. Resting platelets were permeabilized with 0.75% Triton X-100 and 0.1% glutaraldehyde and 5 μM phallacidin in PHEM buffer (9, 30). The cytoskeletons were pelleted onto the surface of a glass coverslip, washed in distilled water, rapidly-frozen, freeze-dried, and rotary-coated with platinum and carbon. Permeabilization, followed by centrifugation, separates the total membrane skeleton (*ms*) from underlying actin cores (*c*). (*a* and *b*) In many cases, the core remains attached to the membrane skeleton. (*d*) In some cases, an oval-shaped actin core is found sitting next to its membrane skeleton. The actin core may also be found fragmented into two parts, a central core and circumferential filament ring (*cfr*). *a*, *b*, and *d* are of the same magnification. (*c*) The circled region in (*d*) of the *cfr* decorates with myosin S1, identifying the filaments as actin. Bar: (*a*, *b*, *d*) 1 μm; (*c*) 0.1 μm.

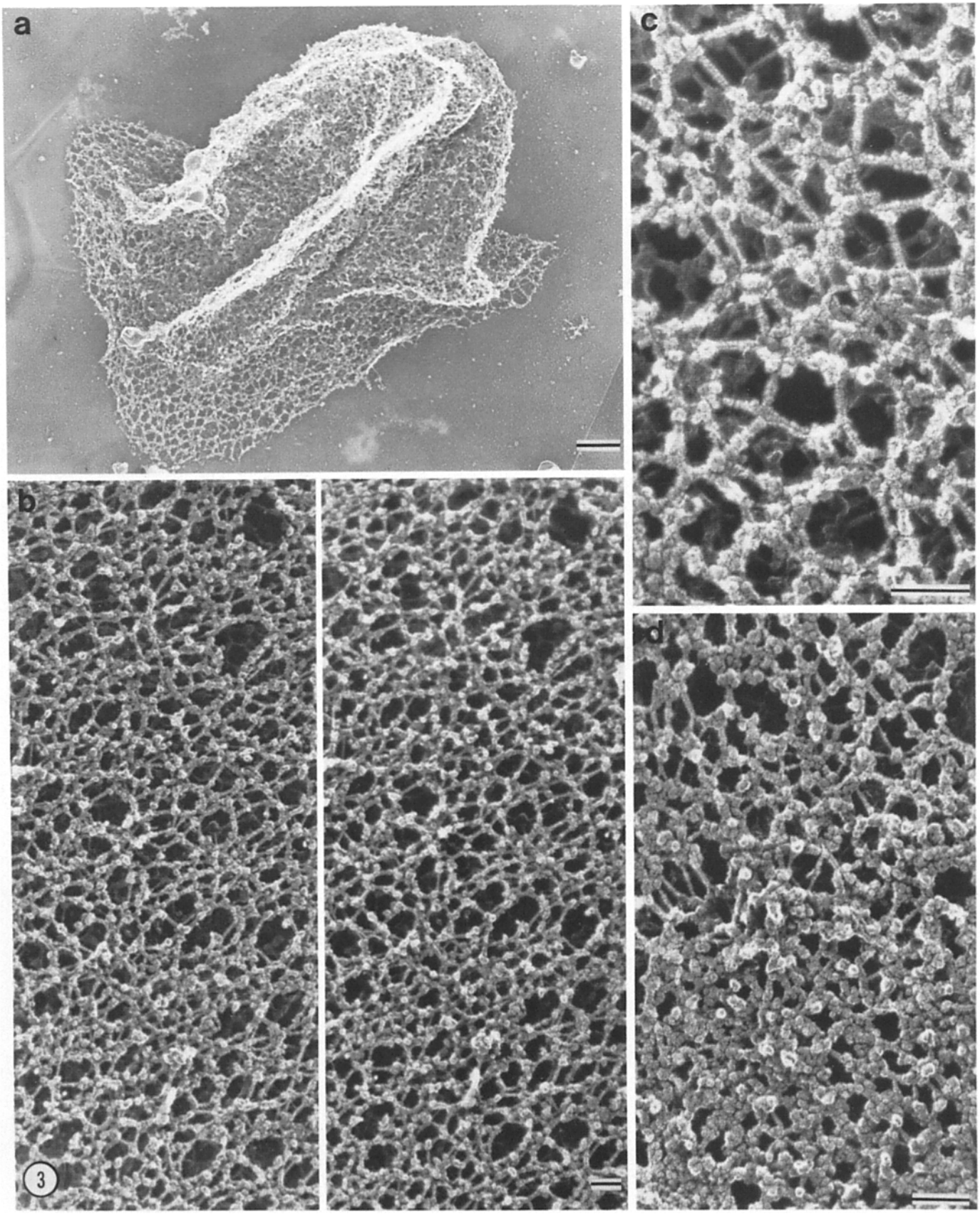

Figure 3. Gallery of micrographs showing the variability in the structure of the membrane skeleton of resting platelets permeabilized in the presence of fixative but without phallacidin. (*a*) Low-magnification electron micrograph showing a representative glass adherent and intact membrane skeleton after permeabilization of cells in PHEM-Triton-glutaraldehyde, centrifugation onto a glass support, rapid-freezing, freeze-drying and metal-coating. The membrane skeleton, which has been separated from its underlying actin filaments (see Fig. 2, above) is a sheet composed of a fibrous network which is not as dense as the residue sheets of total membrane skeleton in the presence of phal-

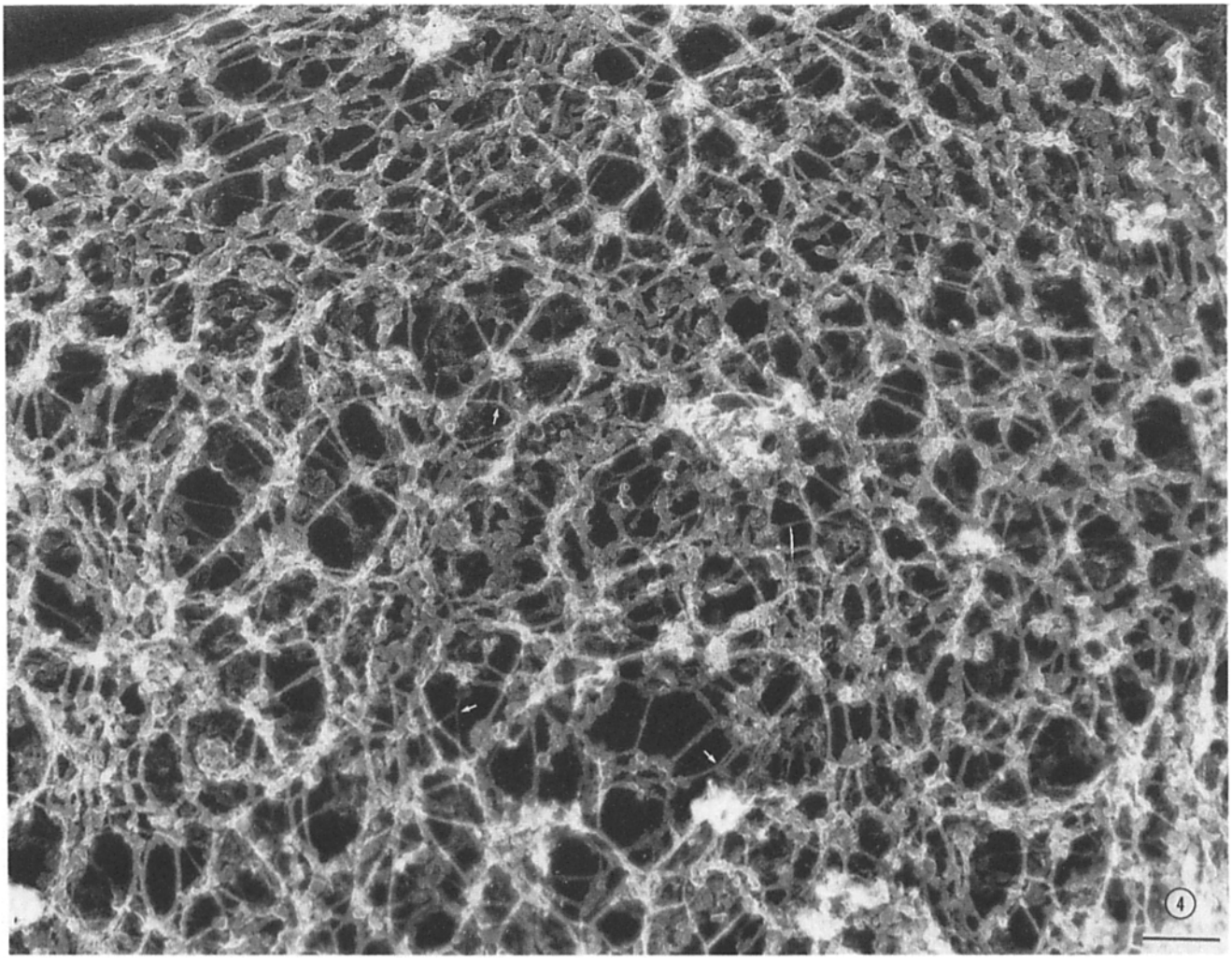

Figure 4. The structure-simplified membrane skeleton prepared from a resting platelet in the absence of fixative and phallacidin. The membrane skeleton permeabilized for 2 min without glutaraldehyde or phallacidin in the extraction solution is a uniform porous sheet composed of long, thin interconnected fibers. Fibers are 4 nm wide, with maximal lengths of 240 nm. They can be observed to bifurcate into two strands occasionally (*arrows*). In general, they interconnect forming triangular-shaped pores. The membrane skeleton has been coated with tautalum–tungsten alloy. Bar, 0.1 μm.

Beckman Instruments, Fullerton, CA). The protein content of the clarified supernatant was determined by total protein assay. The amount of total protein in the cytoskeletal pellet was calculated from the difference between the total platelet protein and the detergent soluble supernatant. The pellet was dissolved with boiling 1% SDS in gel sample buffer and electrophoresed through 5–15% acrylamide slab gels in the presence of 0.1% SDS (12). Protein in the gels was either stained with Coomassie blue or transferred to immobilon for blotting against the various IgGs (38).

Planar Morphology. The length of spectrin strands, the percent area covered by spectrin strands in unfixed membrane skeletons, and the number of anti-GPIb gold particles per squared micrometer of membrane skeletal area was determined using a Microcomp Integrated Image Analysis System (Southern Micro Instruments, Atlanta, GA). The total area of membrane sheet, the total number of gold particles, and the area covered by strands was measured on micrographs of membrane skeletons from cells permeabilized with Triton-PHEM solutions in the absence of fixatives enlarged to a final magnification of 200,000. For the quantitation of anti-labeling, gold particles within a total area of 1 μm^2 were counted in each of five different micrographs.

Results

The Structures of the Resting Platelet Cytoskeleton: Fragmentation into Component Parts

The structure of the detergent-insoluble cytoskeleton of the resting platelet is shown in Fig. 1. In thin sections, cytoskeletons from detergent permeabilized cells retain a discoid shape, showing them to be in a resting state before detergent treatment (Fig. 1 *b*). Fig. 1 *a* shows a representative replica of a platelet permeabilized in identical fashion but processed

lacidin. (*b*) Stereo-paired micrographs of a representative region from a membrane skeleton prepared as described above. Stereo viewing shows this membrane skeleton to be composed of two superimposed layers. (*c*) Higher magnification electron micrograph showing the substructure of the membrane skeleton shown in *b*. It is composed of strandlike elements interconnected by globular particles. Strands have diameters of 7–8 nm. (*d*) Electron micrograph showing the heterogeneity in the density of a membrane skeletons prepared in the absence of phallacidin across its surface. Bars: (*a*) 0.5 μm; (*b–d*) 0.1 μm.

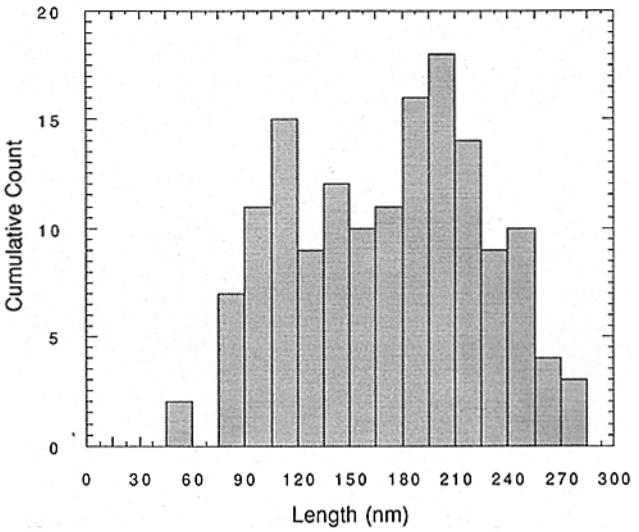

Figure 5. Histogram showing the length distribution of strands measured in maximally extended membrane skeletons (such as shown in Figs. 4 and 10 *a*). Strand length between points of intersection was measured by planar morphology. Strand lengths distributed between two peaks. The first, accounting for 40% of the total, was centered at 116 nm. The second, accounting for the rest of the strands, averaged 210 nm in length.

for the electron microscope by rapid-freezing and freeze-drying. This micrograph demonstrates that resting cytoskeletons have an extremely dense coat capable of completely masking the underlying filaments revealed in the thin sections (Fig. 1 *b*). The only interruptions in this uniform coat are a number of small holes that may correspond to invaginations of membrane forming the pores of the canalicular system in unextracted cells. We designate this structure the total membrane skeleton.

As first proposed by Fox and colleagues (1, 5), the margin observed in thin sections of resting cytoskeletons and in replicas corresponds to the total membrane skeleton. The following experiments demonstrate that this membrane skeleton can be detached from the underlying filaments using mechanical shear and, depending on the conditions of cell permeabilization, separated into derivatives of lesser complexity. Sedimentation of intact cytoskeletons onto the surface of glass coverslips causes them to rupture and resolve into two component parts; spread sheets of membrane skeleton, found adherent to the coverslip surface in a variety of conformations, and cores of interdigitating filaments (Fig. 2). Many free filaments are also scattered abundantly on the coverslip surface. Filamentous cores remain either partially attached to (Fig. 2, *a* and *b*) or nearby (Fig. 2 *d*) the membrane skeleton. In some cases, the filament core further fragments into a central domain composed of radially oriented fibers and a ring of circumferential filaments. This radial array of filaments is distinct from the marginal ring of microtubules in the resting cell. Microtubules separate as an intact ring structure with some associated fibers (data not shown).

The Total Membrane Skeleton of the Resting Platelet

The ultrastructure of the detergent-insoluble planar sheet (the total membrane skeleton) derived from platelet cytoskeletons varies depending on the conditions of cell permeabilization. If glutaraldehyde (0.1–1%) is present during detergent permeabilization, membrane skeletons separate from their underlying filament cores (see below) as spread sheets whose porosity varies from 10 to 150 nm (Figs. 2 and 3). If both glutaraldehyde and 5 μM phallacidin were present during the detergent permeabilization, the membrane skeletons separated by centrifugation from the cores only as dense forms. As shown in Fig. 2, these skeletons are very tightly woven and are very similar in appearance to the membrane skeleton of uncentrifuged cytoskeletons (Fig. 1 *a*). Details on the substructure of these membrane skeletons are best appreciated in membrane skeletons prepared in the absence of phallacidin which are more spread or stretched with pores in the range of 80–150 nm (Fig. 3, *a–c*). Detached membrane skeletons of greater porosity are shown in Fig. 3. In platinum replicas, the substructure is more clearly revealed in stereo (Fig. 3 *b*) and at high magnification (Fig. 3 *c*). The membrane skeleton in Fig. 3, *b* and *c* comes from a region similar to that shown in the middle of Fig. 3 *a* where the top and bottom sheets of membrane skeleton are folded over on themselves. Strands of variable lengths (30–100 nm) having 6–10 nm diameters interdigitate with globular particles forming a flat meshwork. Each globular particle is 10–20 nm in diameter and is generally observed in aggregates of two to five. Regions from membrane skeletons of other cells are very tightly interwoven (Fig. 3 *d*) and are so dense that it is difficult to dissect the individual strand elements from the globular particles observed in the more open forms (Figs. 1, 3 *d*, and 9 *a*). In the more open skeletons, strands composing the struts are dotted periodically with both single and clustered globular particles. In general, particles cluster at points where the strand-like elements intersect or abruptly alter their course.

The Simplified Membrane Skeleton

A clearer picture of the composition and interconnection of strands forming an intrinsic meshwork is revealed in maximally porous specimens that can be prepared from cells permeabilized in the absence of fixatives and phallacidin and which we designate the simplified membrane skeleton. Figs. 4 and 9 *a* show representative tantalum–tungsten replicas of the simplified membrane skeleton from a resting platelet permeabilized with detergent buffers lacking these stabilizing agents. The simplified membrane skeletons in these preparations are uniform in appearance and porosity. Relative to the dense sheets described in Figs. 1, 2, and 3 *d*, they have a markedly increased pore size of ~100–250 nm which

Figure 6. Sequence of electron micrographs showing how actin filaments attach to the total membrane skeleton. Total membrane skeletons were prepared, fixed, and adhered to a glass surface as described in Fig. 1. They were then treated for 5 min with the rabbit skeletal muscle S1, unbound S1 removed by washing, and the membrane skeletons were then fixed in 1% glutaraldehyde, 0.2% tannic acid, 10 mM sodium phosphate buffer for 10 min, washed into water and rapidly frozen. Myosin S1 labeled filaments acquire the appearance of twisted cables

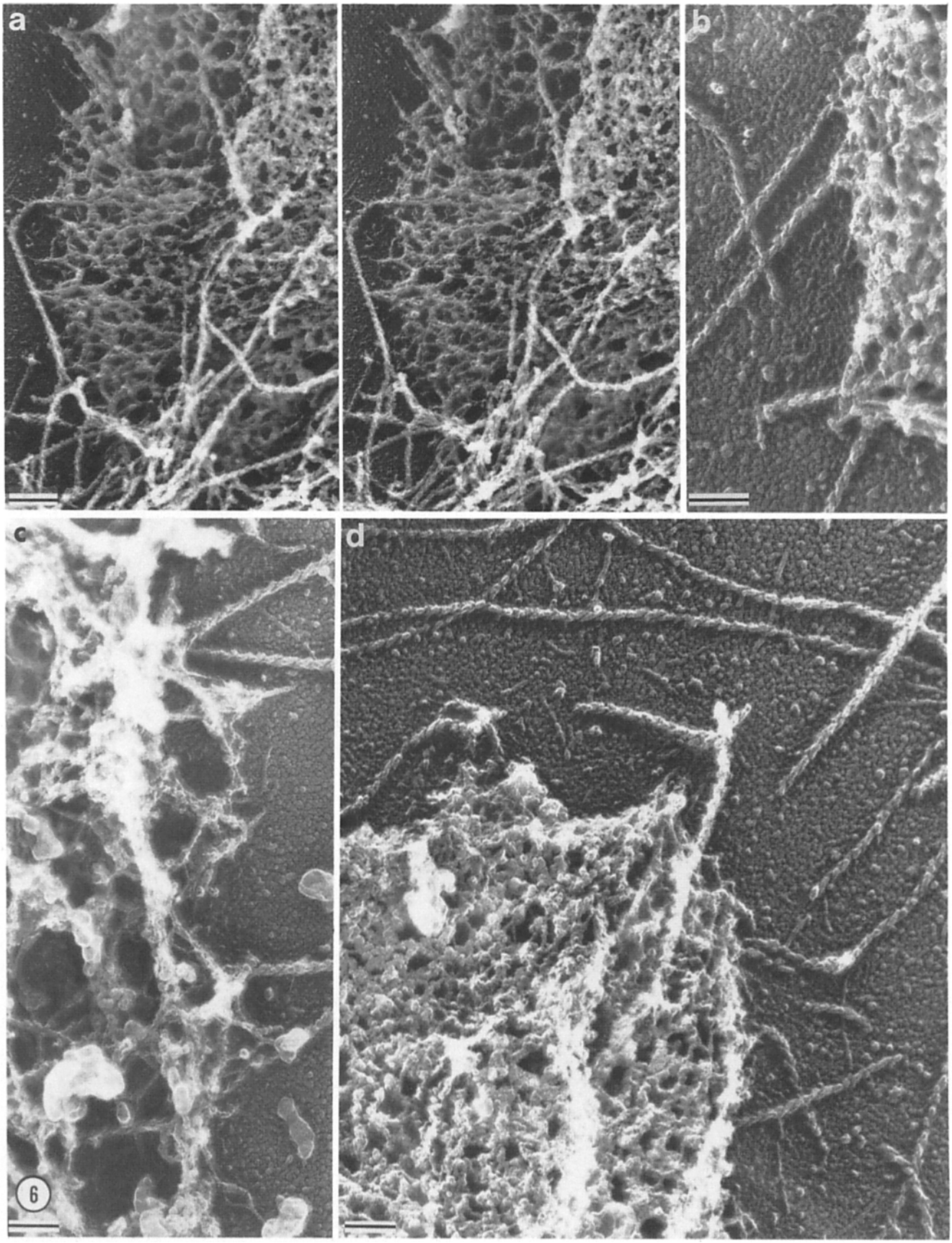

in which pointed and barbed ends can be defined. The interaction of actin filaments with the total membrane skeleton occurs in two ways: (*a*) at their ends through multiple strand-like connections and (*b*) along their sides through similar strand-like connections. In both cases, filaments are attached by strands having dimensions similar to those forming the planar membrane skeleton. Bars: (*a*) 0.2 μm; (*b–d*) 0.1 μm.

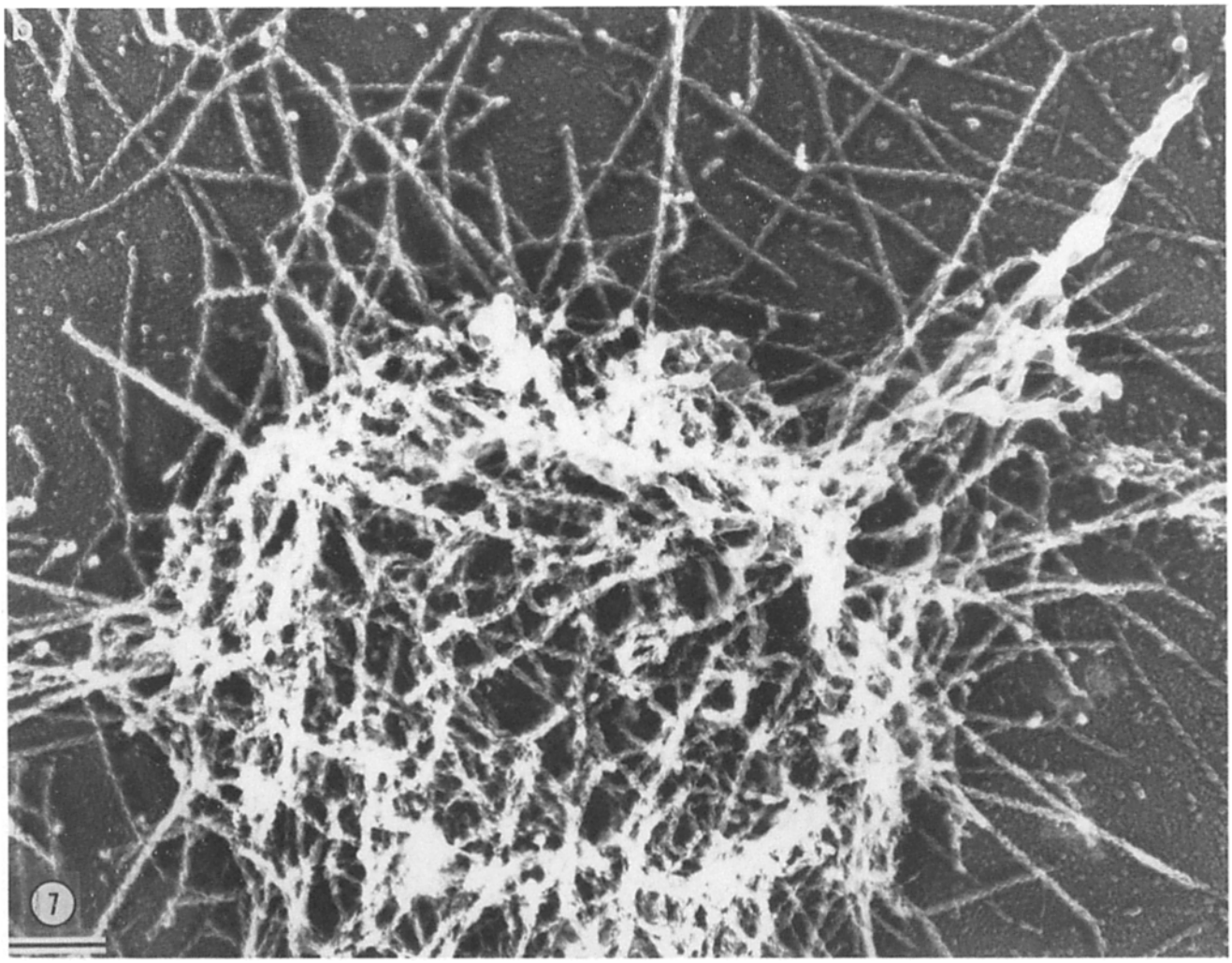

Figure 7. Demonstration that the filamentous core of the resting platelet is composed of actin filaments. When cytoskeletons from resting cells permeabilized in the presence of 0.1% glutaraldehyde and 5 μM phallacidin are sedimented onto a coverslip, individual actin filaments and a filamentous core are dispersed across the surface of the coverslip. Individual filaments and those comprising the core were identified by labeling with myosin S1. For each sheet of membrane skeleton, a three-dimensional core of actin filaments was found either sitting in close apposition with some filaments remaining attached to or detached and in close proximity to a membrane skeleton. Cores were spherical to oval in shape when viewed in stereo micrographs, and as shown here, composed almost entirely of actin filaments. Actin filaments having free ends radiate outward from the cores and in some cases (Fig. 2 *b*) make direct connections with the membrane skeletons (Fig. 6). Radially oriented filaments have both their pointed or barbed filament ends exposed. Bar, 0.2 μm.

derives, at least in part, from an increase in the surface area to ~200% of the total membrane skeleton prepared with fixative and phallacidin. The maximum diameter of resting platelets measured in thin sections was 3.2 ± 0.4 μm (mean ± SEM, n = 50). Cytoskeletons prepared by permeabilizing resting cells in the presence of fixative and phallacidin were of similar size as intact cells measuring 2.8 ± 0.1 μm (n = 100) in their maximal dimension both in thin sections or in metal replicas (Fig. 1 *b*). Cytoskeletons from cells permeabilized in the absence of fixative and phallacidin were, however, always >4 μm across their longest dimension (4.2 ± 0.2 μm, n = 50) indicative of an extension during detergent permeabilization. Importantly, the membrane skeleton separated from these unfixed cytoskeletons was morphologi-

Figure 8. Localization of spectrin in the detergent insoluble cytoskeleton and in the total and simplified forms of the platelet membrane skeleton. (*a*) Cytoskeletons from resting cells were embedded in Lowicryl K4M and thin sectioned. (*b–d*) Membrane skeletons were permeabilized in the presence (*b*) or absence (*c*, *d*)) of glutaraldehyde and phallacidin. Thin sections and glass adherent cytoskeletal preparations were reacted with affinity purified rabbit anti-spectrin antibody followed by 8-nm gold particles coated with goat anti-rabbit antibody. (*a*) In thin sections, spectrin locates both near the cytoskeletal margins (the membrane skeleton) and in the cytoskeletal interior. (*b*) Anti-spectrin gold densely coats the total membrane skeleton but does not label the actin filament core (*c*, *d*) Anti-spectrin antibodies heavily stain many of the strand components forming the struts of the simplified membrane skeleton. Bars, 0.2 μm.

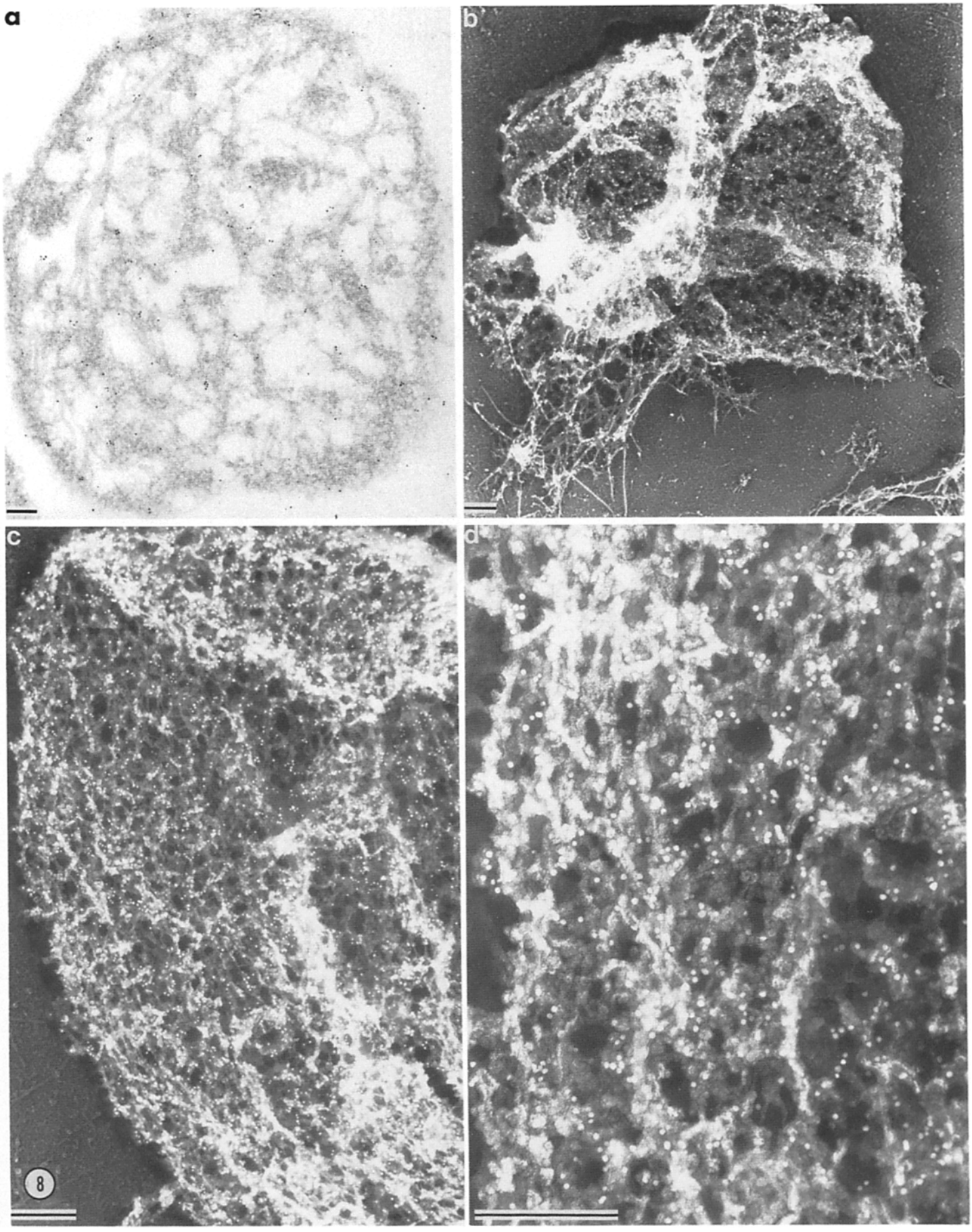
a
b
c
d
8

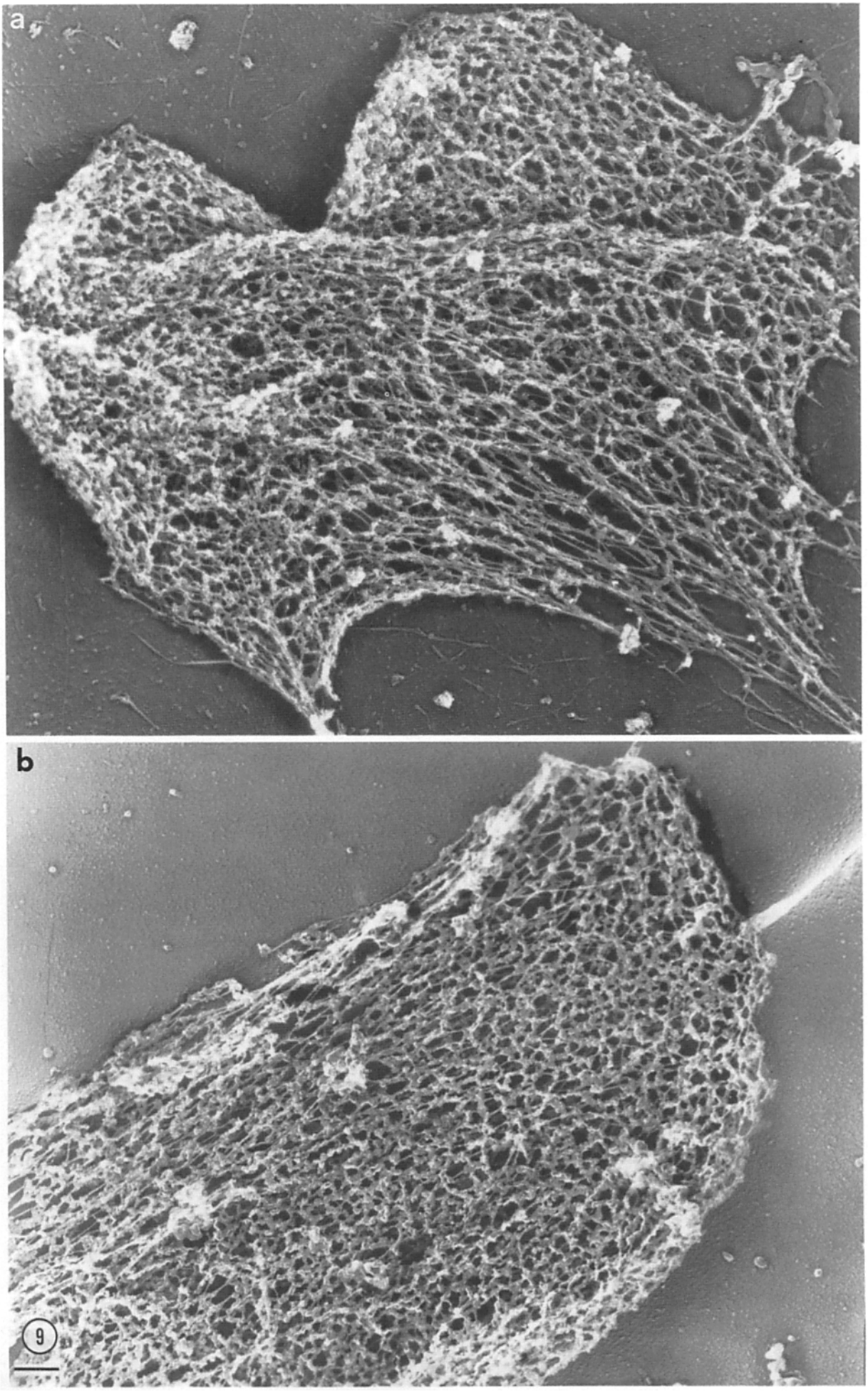
a
b
9

cally simplified. The membrane skeletons were more uniform in ultrastructure and composed of thin strands 4–5 nm in diameter connected at intervals by globular particles. In many cases, thin strands interconnect forming triangular shaped pores. The lengths of the thin strands between particles measured in micrographs such as Figs. 4 and 9 *a* segregated around two averages: one at 210 nm (60% of total) and another (40%) at 116 nm (Fig. 5). Since strand lengths are between intersections, which are in turn defined by associated particles, the maximal strand subunit length is on the order of 200–250 nm. Shorter intersection lengths result from the midpoint decoration of strands with other more globular components and also from points where strands make crossings. In many cases, thin strands can be observed to bifurcate, suggesting that they are composed of at least two elongated subunits. Thicker strands observed in specimens of the complete lamina may be composed of side-by-side alignments of these 4–5-nm-wide thin strands. To estimate the area covered by thin strands, we used planar morphometry to determine the total surface area of 10 of the simplified membrane skeletons and then measured the amount of this area covered only by thin strands. This approach indicated that ~5% of the total area of the simplified membrane skeleton was covered by thin strands.

Connection of Actin Filaments with the Total Membrane Skeleton

We examined the interaction of actin filaments with the membrane skeleton using myosin S1 to decorate the filaments with arrowhead complexes (Figs. 6 and 7). Although long actin fibers are not identified by myosin S1 decoration in the total membrane skeleton or its derivatives prepared from cells permeabilized using detergent lacking fixative and phallacidin, long actin fibers make connections at one end with the surface and margins of the total membrane skeleton (Fig. 6), and at their other ends interconnect to form oval cores (Figs. 2 and 7). The gallery of micrographs in Fig. 6 (and Fig. 2) shows how actin fibers connect to the membrane lamina. Myosin S1-decorated actin filaments 0.5–1 μm in length present either their barbed or pointed ends to the cytoplasmic surface of the membrane skeleton where in many cases they are attached by elongated strands which derive from the membrane skeleton (Fig. 6 *b*). Strands connecting the actin filaments have the same 4–5-nm widths as the main component of the simplified membrane skeleton (Fig. 6 *b*). Actin filaments also come into close association with the membrane skeletons along their sides, i.e., filaments orient parallel to the surface of the membrane skeletons and appear to be similarly connected at multiple points on their sides (Fig. 6 *a*). Fig. 6, *c* and *d* show many barbed filament ends arriving at the membrane skeleton. Fig. 7 shows that the filaments composing and radiating outward from the cores are also primarily actin (as in Fig. 6). Individual actin filaments were also distributed across the coverslip surface in specimens permeabilized in the presence of phallacidin and fixative (Fig. 2 *c*).

Composition of the Simplified Membrane Skeleton

Many of the strands composing the simplified membrane skeleton are nonerythroid spectrin because they are highly labeled with anti-spectrin IgGs and gold particles but not other antibodies (see below). As shown in Fig. 8, anti-spectrin gold densely labels both the total membrane skeleton (Fig. 8 *b*) and along the sides of the strands forming the struts of the simplified membrane skeleton (Fig. 8 *c* and *d*). Gold labels the sides of strands which have been thickened with a uniform coating of antibody. Anti-spectrin gold also labeled the edges and interior of cytoskeletons in thin sections (Fig. 8 *a*) but did not label the sides of actin comprising the filamentous core of the resting cell (Fig. 8 *b*). Labeling was specific for anti-spectrin antibodies. Removal of anti-spectrin antibody during the labeling procedure resulted in the absence of gold labeling of membrane skeletal components (data not shown) and a variety of other antibodies did not label the strand component. A remarkable similarity in overall structure of the simplified platelet membrane skeletons to spread planar spectrin–actin meshes of red cells prepared for the electron microscope by the same technique was also apparent (Fig. 9).

Since the bulk of the strands forming the simplified membrane skeleton are spectrin, these spectrin polymers must interconnect using other platelet components. Based on our understanding of the membrane skeleton of the red blood cell, it is likely that actin oligomers or filaments serve as a junction. Actin filaments are observed to attach along the surface of and at their ends to the total platelet membrane skeleton. These attachments are mediated by thin strands similar in structure to the spectrin strands of the simplified membrane skeleton (Fig. 7). To test whether long actin filaments were required for the integrity of the platelet membrane skeleton, cytoskeletons were incubated with calcium and high concentrations of purified plasma gelsolin, a protein that binds to and severs actin filaments. These conditions failed to disrupt the integrity of the simplified membrane skeleton although they completely disrupted the actin filament cores in the cytoskeletal samples (data not shown).

One mechanism shown to connect cytoskeletal actin to the platelet membrane in the resting platelet is the GPIb-ABP complex (2, 3, 25). In confirmation of earlier studies (5), anti-GPIb gold binds strongly to the surface of the total membrane skeleton separated from cells permeabilized in the presence of fixative and phallacidin (Fig. 10 *a*). The gold particle density per squared micrometer of membrane surface was 702 ± 86 (mean + SE, $n = 5$). However, anti-GPIb gold labeling of the simplified membrane skeleton was drastically reduced relative to the total skeleton (Fig. 10, *b* and *c*). Gold label on the simplified membrane skeleton took the form of individual particles and small aggregates composed of two to four particles. Particles rarely decorated the sides of the spectrin strands in the simplified membrane skeleton and were restricted to particulate material at points where the strands intersected. The gold particle density across the surface of the simplified skeleton was 84 ± 13

Figure 9. Comparison of the structure of the simplified platelet membrane skeleton (*a*) to the erythrocyte membrane skeleton (*b*). Cytoskeletons from both cell types were prepared as in Fig. 4. The magnifications of *a* and *b* are the same. Bar, 0.2 μm.

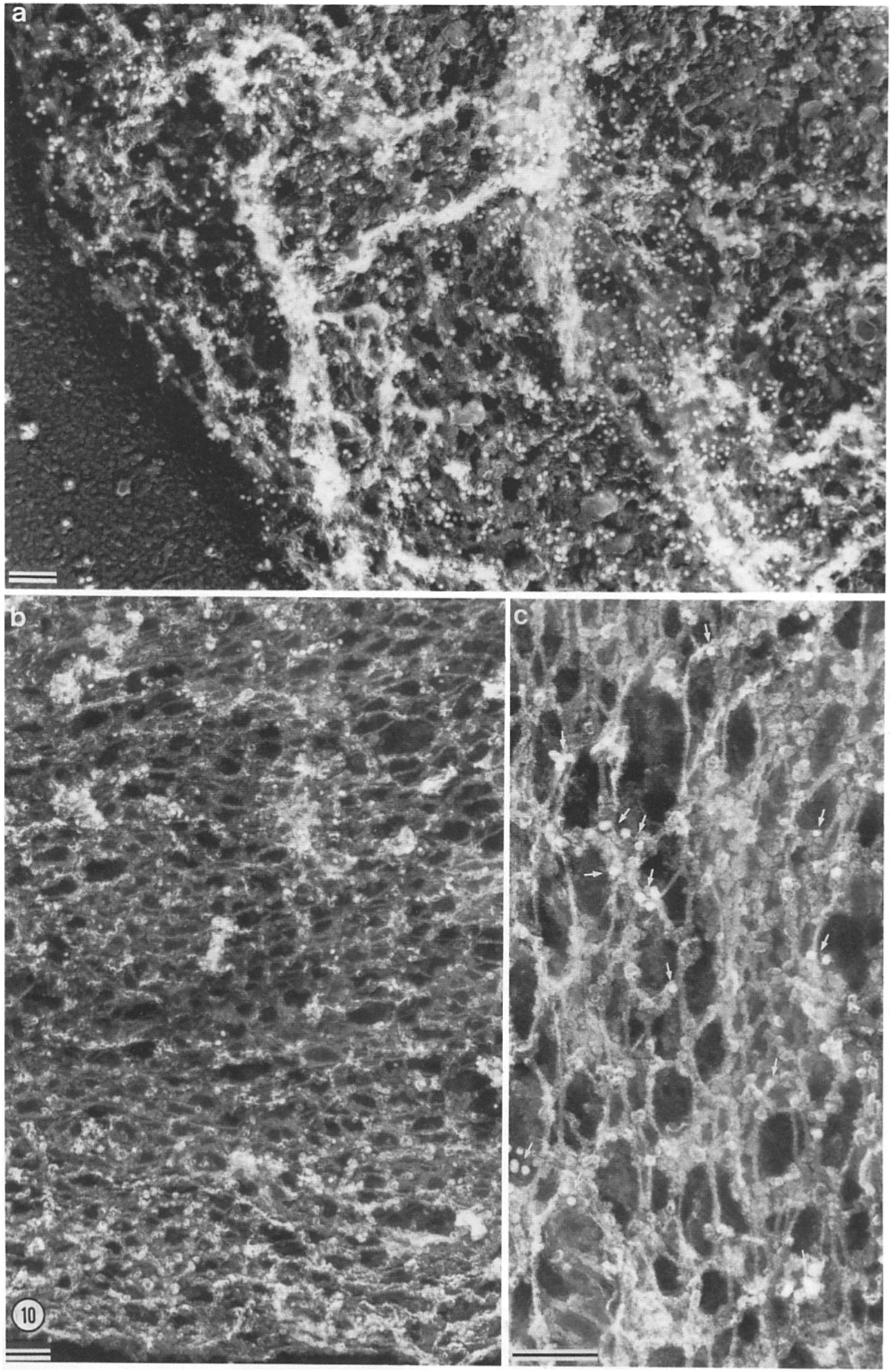
a
b
c
10

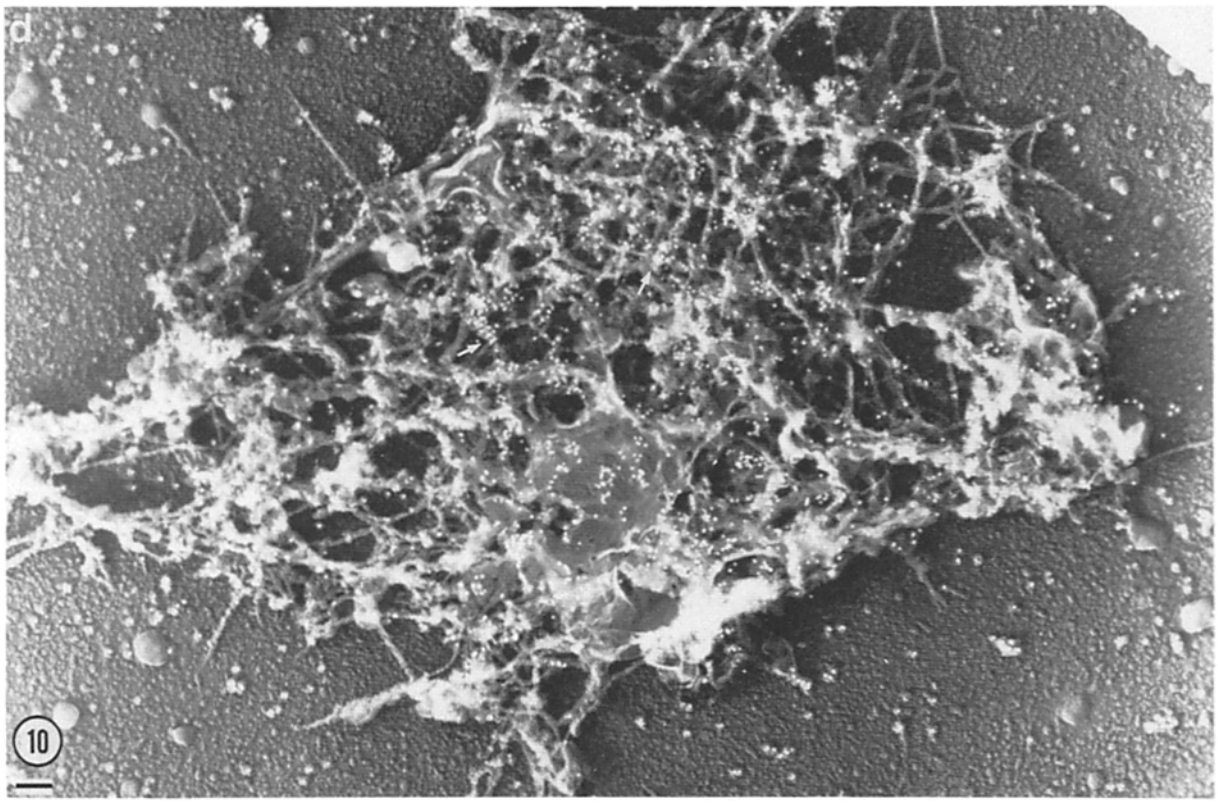

Figure 10. Localization of GPIb in a resting platelet membrane skeleton. (*a*) Fixed membrane skeletons adhered to glass surfaces were treated sequentially with a mouse monoclonal IgG against human GPIb and 15 nm gold particles coated with rabbit anti-mouse IgG. Strong labeling of the total membrane skeleton with gold particles is apparent, although it is not possible to define which elements are being labeled. (*b*) Localization of GPIb in membrane skeletons separated from their underlying actin core in the absence of fixative. In marked contrast to the fixed skeletons, simplified skeletons contain little GPIb as demonstrated by the marked reduction in gold label in these specimens. (*c*) High magnification of a simplified membrane skeleton after labeling with anti-GPIb antibody. The arrows indicate gold particles. (*d*) Localization of GPIb in an actin core separated in the absence of fixative. Considerable anti-GPIb gold remains in actin cores detached from the membrane lamina. Note that gold particles are linearly aligned on the surface of actin filaments (*arrow*). Bars, 0.1 μm.

(mean $\pm$ SE, $n = 5$). Since simplification of the membrane skeleton increased its surface area from an average of 14–27 squared microns, the total number of gold per membrane skeleton was 9,828 (702 gold/squared microns $\times$ 14 squared microns) versus 2,268 (84 gold/squared microns $\times$ 27 squared microns). 77% of the GPIb/IX complex, therefore, is removed during the conversion of the total membrane skeleton to its simplified form.

Since most of the GPIb/IX complexes (70–90% of the total) in resting platelet are bound to actin filaments via ABP (2, 3, 25), the depletion of GPIb antigen as the total skeleton is converted into the simplified form could result from disassembly of actin fibers or dissociation of ABP molecules from GPIb/IX complexes or ABP/GPIb/IX complexes from actin filaments. Anti-GPIb gold label in cytoskeletons prepared without fixative or phallacidin, however, strongly labeled the actin filaments in the three-dimensional core of the resting cell. Figure 10 *d* shows that anti-GPIb gold densely labels cytoskeletal cores separated from cells permeabilized in the absence of fixative. Only sparse labeling with anti-GPIb gold was observed in cores detached in the presence of fixatives (data not shown). Therefore, mechanical shearing of unstabilized cytoskeletons separates at least some actin filaments having bound ABP/GPIb/IX complexes, a process that may contribute to the simplification of the membrane skeleton.

Anti-ABP gold, on the other hand, labels both forms of the membrane skeleton sparsely in the form of small clusters of two to three gold particles which are widely spaced across the membrane skeletal surface, but densely labels the actin filament cores (Fig. 11, *a* and *b*). Gold labeling in the actin cores was in the form of extended aggregates of 15–20 gold particles intertwined around filament intersections, and along the sides of the filaments radiating outward from the core (Fig. 11 *c*). The weak labeling of the membrane skeleton does not appear to result from inaccessibility of ABP molecules to anti-ABP antibodies, as anti-ABP gold densely labels the margins of both intact cells and cytoskeletons in thin sections.

An additional component of the simplified membrane skeleton is myosin. As shown in Fig. 12, anti-myosin IgG gold densely stains the rim of platelet cytoskeletons in thin sections as well as locating within the actin core of cells. Labeling of separated membrane skeletons took the form of periodic groups of two to four clusters of gold particles (Fig. 12 *a*), spanning a total length of $\sim$200 nm. If myosin is a

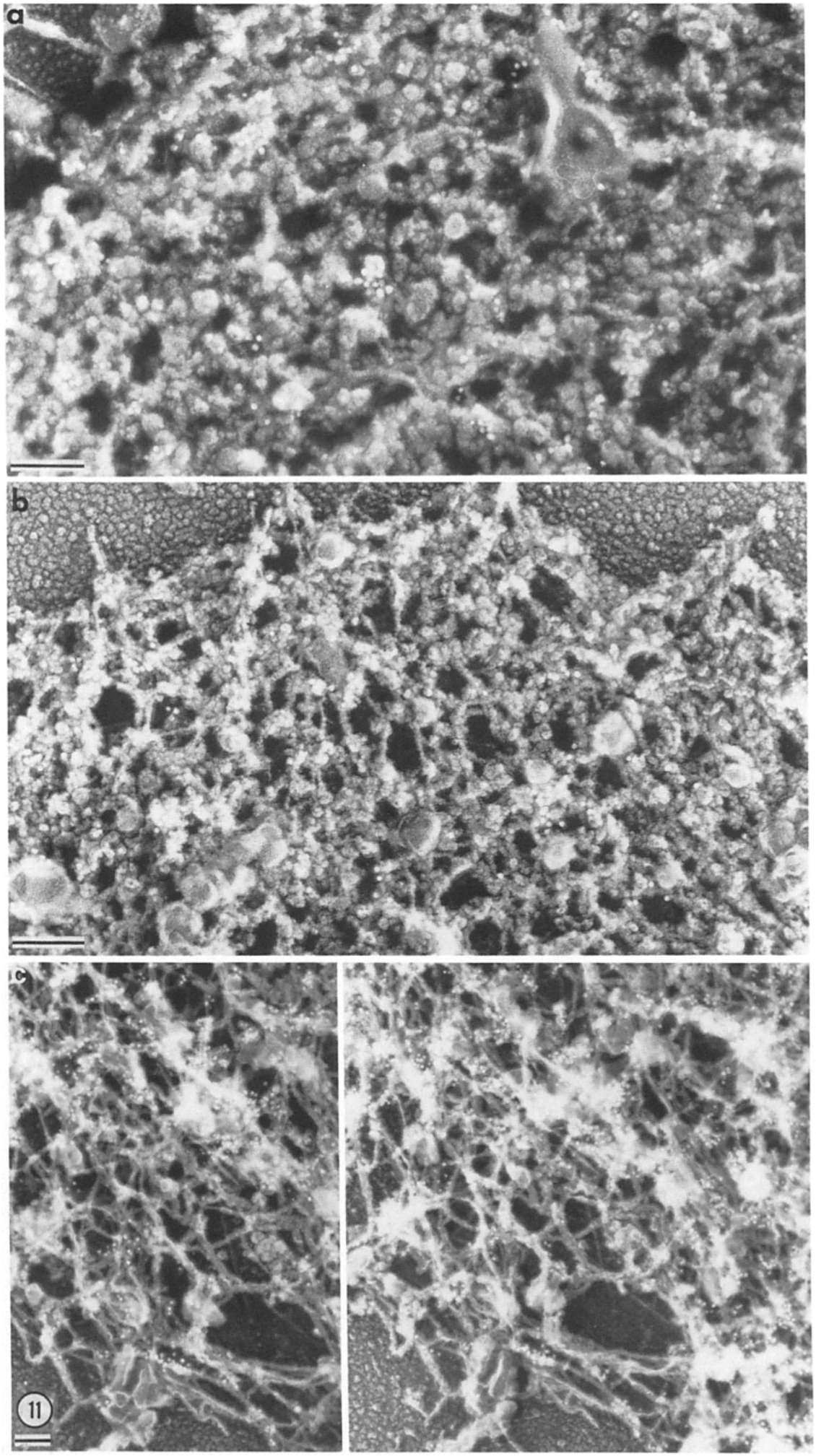
a
b
c
11

major component of the membrane skeleton, it does not appear to be held in place by attaching to short actin filaments, because incubation and washing of membrane skeletons with 5 mM ATP in PHEM buffer, which should dissociate actin–myosin complexes, had no effect on their structural integrity (data not shown).

The Polypeptide Composition of the Resting Platelet Cytoskeleton

Identification of spectrin as a component of the simplified membrane skeleton by immunoelectron microscopy indicated that it should be enriched in cytoskeletons, particularly under the extraction conditions promoting the formation of the simplified membrane skeleton. Fig. 13 shows the polypeptide composition of 5–15% gradient SDS-PAGE of resting platelets and of cytoskeletons from these cells after permeabilization using PHEM-Triton X-100 solutions. Platelets contain major Coomassie-blue stainable polypeptides at 270, 235, and 200 kD reported to correspond to ABP, talin (sometimes designated p235), and myosin, respectively (24, 27, 28, 31). ABP and P235/talin are enriched approximately twofold in cytoskeletons relative to their distribution in total cellular extracts while myosin is only slightly enriched in the cytoskeletal fraction. Immunoblotting for spectrin in the samples reveals that although there is a modest increase in 235-kD polypeptide in the cytoskeletal fraction, anti-spectrin antibody reactive protein(s) in the P235 region is highly enriched relative to intact cells and that under these SDS-PAGE conditions spectrin polypeptides comigrate with talin. Fox et al. (6) has previously shown that resolution of the spectrin polypeptides required extended electrophoresis times.

Discussion

Our high-resolution views of the cytoskeleton of the resting platelet have revealed it to be composed of a dense two-dimensional membrane skeleton connected to a core composed predominantly of actin filaments. The resting platelet cytoskeleton, therefore, resembles a spoked wheel in which a highly crosslinked three-dimensional oval-shaped actin filament core is the hub of the wheel and the two-dimensional membrane lamina its rim (Fig. 14). The hub and rim are joined by spokes of radially oriented actin filaments. The localization of ABP at filament crossover points in the core suggests that ABP plays a major role in stabilizing and defining its three-dimensional structure. This spoked wheel configuration has been inferred from immunofluorescence in bovine platelets (37) and observed occasionally in thin sections (1). The membrane meshwork is a striking structure which, if strongly coherent and held taut by the underlying actin filaments of the resting cell, might account for the toughness of the circulating platelet.

Composition of the Membrane Skeleton

The total membrane skeleton contains distinct, but integrated fiber systems. One of these is a framework of elongated, thin strands connected at globular nodes. Ultrastructural immunocytochemistry showed that many of the strands are spectrin as anti-human brain spectrin antibodies labeled many of the strands uniformly along their lengths. Other evidence suggests spectrin molecules are in the tetrameric form. First, their 4 × 210–240 nm dimensions are near that predicted for those of nonerythroid spectrin tetramers (8, 19). Second, strands were observed to occasionally resolve into two thinner fibers identical to separations which have been observed between the chains of spectrin tetramers on the cytoplasmic surface of negatively stained red cell membrane fragments (15, 32) and along purified tetramers displayed on mica and rotary shadowed (8, 39). Lastly, the platelet membrane skeleton can be simplified into a porous meshwork virtually indistinguishable from the spectrin–actin lamina of erythrocytes when it is prepared by the same techniques. In thin sections, anti-spectrin gold was enriched near the margins of cytoskeletons and also present in the cytoskeletal interior. The internal labeling may represent spectrin which lines the cytoplasmic face of the internal canalicular system of the resting cell.

From the amount of area covered by spectrin strands in the simplified membrane skeleton, the number of spectrin tetramers necessary to assemble such a contiguous structure can be estimated. We determined that ~5% of the surface area of a simplified membrane skeleton was covered by these strands. Since the simplified membrane skeleton averaged ~4.25 μm in their longest dimension, we calculate the surface area of a simplified membrane skeleton to be ~27 μm^2. The area of the simplified membrane skeleton covered by spectrin is therefore ~0.67 μm^2 into which 1,100–1,300 spectrin dimers could fit using molecular dimensions of 3–5 × 120 nm (8). Therefore, from these morphological analyses, 550–750 spectrin tetramers are required to assemble the simplified membrane skeleton. What percent of the total platelet protein need be spectrin if there are 750 spectrin tetramers? Since 100 mg of platelets is 2.4×10^{11} cells, each cell would contain 4.1×10^{-13} g of protein. If all this protein is spectrin tetramer there would be $\sim 2.5 \times 10^5$ molecules of tetramer in a cell (4.1×10^{-13} g/l × 10^6 mol wt = 0.41×10^{-18} mol; × 6.023×10^{23} molecules/Mole = 2.46×10^5 molecules). For 750 tetramers per cell, therefore, 0.3% of the total platelet protein should be spectrin. This is near the concentration at which spectrin is believed to be present in a platelet (22). A concentration of 50 tetramers per squared micrometer of platelet surface area is, however, considerably less than that in erythrocytes where 700 spectrin tetramers are present per squared micrometer of surface area (26).

The second membrane skeletal system is the previously

Figure 11. Localization of ABP in the membrane skeletons of the platelet (*a*, *b*) and in the filamentous actin core (*c*). ABP is visualized in the total membrane skeleton (*a*), the simplified membrane skeleton (*b*) or the actin filament core (*c*) using affinity purified goat anti-ABP IgG and rabbit anti-goat IgG-coated 8-nm gold particles. As shown in stereo-paired micrographs (*c*), the anti-ABP gold particles label points of actin filament intersection in the core and along the sides of F-actin spokes radiating from the core. Weak labeling of both forms of the membrane skeleton is observed although the total membrane skeleton labels to a greater extent than the simplified skeleton. Bars, 0.1 μm.

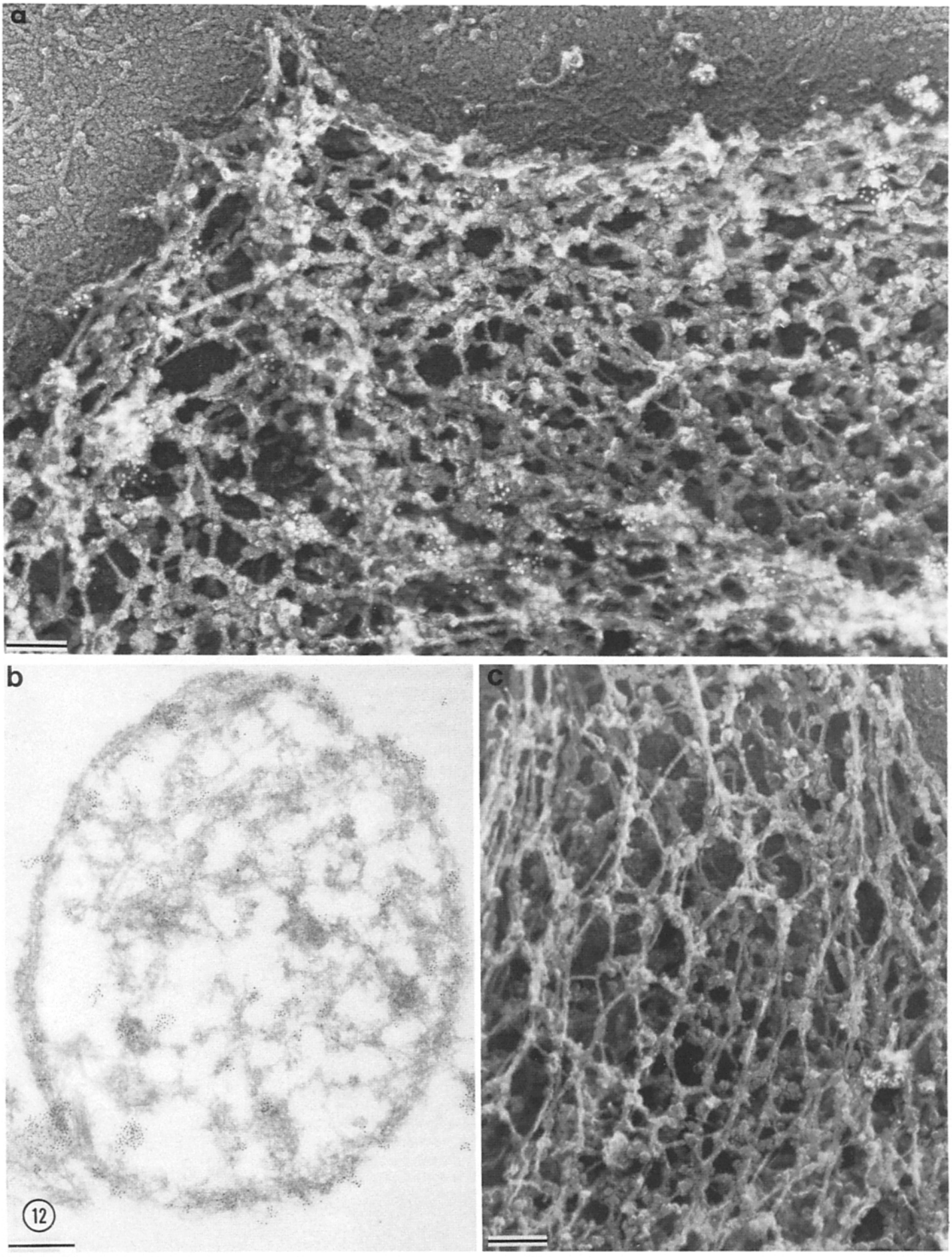
a
b
12
c

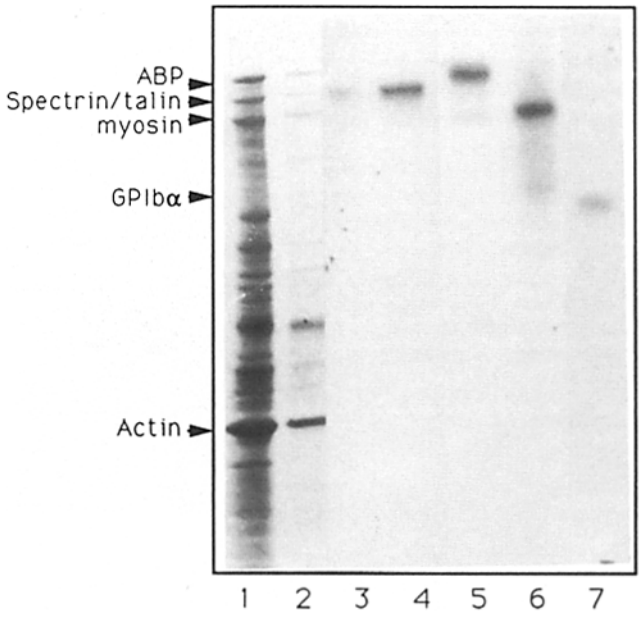

Figure 13. Polypeptide composition of resting platelets and cytoskeletons prepared from these cells. Polypeptides were displayed by SDS-PAGE and transferred to immobilon paper for Coomassie blue staining (*1*, *2*) or immunoblotting with antibodies followed by ^{125}I-anti-primary IgG (*3–7*). (*1*) Intact cells; (*2*) cytoskeletal preparation; (*3–7*) radioautographs of intact (*3*) or cytoskeletal (*4–7*) preparations after staining with rabbit anti-human brain spectrin antibody (*3*, *4*), goat-anti-ABP antibody followed by rabbit anti-goat IgG (*5*), goat-anti-myosin antibody followed by rabbit anti-goat IgG (*6*), and mouse anti-GPIb antibody (*7*). Bound IgG was visualized with ^{125}I-goat anti-rabbit IgG or ^{125}I-rabbit anti-mouse IgG.

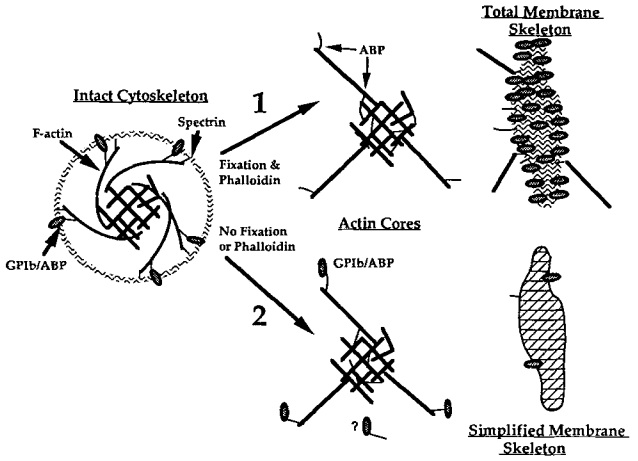

Figure 14. Diagram summarizing the differences in the two types of membrane skeletons. The resting cytoskeleton is composed of a membrane lamina connected to underlying actin filaments. Depending on the method of cell permeabilization, the platelet membrane skeleton was separated from its underlying actin core either as (*1*) the total membrane skeleton, or as a (*2*) simplified membrane skeleton. (*1*) The total membrane skeleton is separated when cells were permeabilized with detergent in the presence of glutaraldehyde and phallacidin. It contains the spectrin-based meshwork of the simplified membrane skeleton but also retains the bulk of the plasma membrane GPIb and some actin filament connections. The bulk of the F-actin in the resting cells dissociates as a filamentous core highly crosslinked by ABP molecules. At least one of the membrane skeleton-actin connections is broken when the membrane skeleton is sheared from the core. The small amount of ABP crossreactive gold labeling suggests that the ABP-GPIb association is broken. (*2*) The simplified membrane skeleton, prepared without fixative or phallacidin, is spectrin rich but GPIb-poor. Some GPIb remains associated with the actin core in the preparations.

identified GPIb/IX-ABP–actin complex. The relationship of this complex to the spectrin-enriched simplified membrane skeleton may explain how conversion of the total membrane skeleton into the simplified one occurred in our studies. Conversion of the dense membrane coat of the resting platelet to the simplified spectrin-stranded meshwork occurs with a concurrent reduction in membrane skeletal-associated GPIb and a ~100% increase in the surface area of the membrane skeleton. The sparse anti-ABP but abundant anti-GPIb gold labeling of membrane skeletons detached from their cores in fixed specimens (Fig. 11) indicates that the GPIb/ABP bond may be broken when the membrane skeleton is mechanically sheared from these underlying actin filaments. In cores separated from unfixed cells, however, this bond appears to remain intact, connecting the GPIb/IX complex to the actin filaments composing it. The increased porosity of membrane skeletons observed in the absence of fixatives and phallacidin suggests that strands could slide across one another in the plane of the membrane or uncoil (17) but are restricted in doing so by the core filaments attached by ABP to GPIb/IX complexes. The opening of the spectrin-based meshwork may occur passively after severing of the underlying actin filaments or might possibly require, in addition, mechanical forces. Expansion of the membrane skeleton may be possible because the GPIb/IX-ABP-actin system is positioned in the membrane such that it can control the porosity of the spectrin-based meshwork. Approximately 25,000 copies of the GPIb/IX complex are present in the plasma membrane of the resting cell (7, 18) tightly linked to ABP (2, 3) and thus, to the underlying actin filaments. The GPIb/IX complex is of sufficient size so that it may physically restrict the mobility of spectrin strands. In the electron microscope GPIb complexes are barbell shaped, 60 nm long having more globular end domains of unequal sizes, the larger being 16 nm, the smaller, 9 nm across (4). The large globular domain has been shown to be the glycocalicin portion exposed on the outside of the cell. This domain may correspond to the many 10–20-nm particles clustered on the

Figure 12. Localization of myosin in the platelet membrane skeleton. (*a*) Membrane skeletons were incubated with affinity-purified goat anti-myosin IgG followed by 5-nm gold particles coated with rabbit anti-goat IgG. Gold label is found as large clusters each containing 5–25 particles. Groups of clustered gold particles (two to four) further align in linear arrays, ~200 nm long. The strand component of the membrane skeleton is not labeled with anti-myosin antibody. (*b*) Anti-myosin labeling in Lowicryl-embedded, thin-sectioned resting platelet cytoskeletons. (*c*) Control in which myosin-absorbed primary IgG was used. Bars, 0.2 μm.

surface of the membrane skeleton. In the total membrane skeleton, the elongated GPIb/IX complexes connected to underlying actin filaments in the pores of the spectrin meshwork might hold the spectrin-based meshwork in a compressed state. Unlocking of these restrictions imposed by the transmembrane GPIb/IX/ABP/actin filament complex may be necessary to form cytoplasmic extensions at the periphery of activated cells.

Other Components of the Membrane Skeleton

Previous biochemical studies have shown that material sedimented at low speed from Triton-extracted resting platelets contained mainly actin, ABP, and GPIb/IX with smaller and variable amounts of α-actinin, tubulin, myosin, talin, GPIV, and GPIα. Since the sedimenting structures presumably included the membrane skeleton, the microtubule ring, the actin core and its radial filaments and undoubtedly molecules trapped with this core, these results are not inconsistent with our model of the platelet cytoskeleton based on the ultrastructural and histochemical data.

One additional component that we demonstrated to be associated with the membrane skeleton was myosin. The surface labeling of myosin confirms our earlier studies where myosin labeling was increased relative to the cytoplasm near the plasma membrane of the resting gel-filtered platelets (33). Myosin represents 1–2% of the total platelet protein, but we previously demonstrated that only about 10% of it was intimately associated with the platelet plasma membrane (33). Anti-myosin gold label in replicas of membrane skeletons was found as groups of gold clusters, a labeling pattern compatible with the length of myosin molecules. Platelet myosin molecules are thin and long (~200 nm) with head regions that would appear as globular particles. Myosin molecules can also assemble into bipolar filaments 300 nm long, therefore, it is possible that myosin at the membrane of the platelet was in the form of small bipolar filaments. How myosin is anchored in the membrane skeleton is unclear as its distribution was not effected by treatment with 5 mM ATP, which dissociates myosin from actin fibers. One possible role of myosin at the membrane would be to impose contractile tension on actin filaments connected to GPIb/IX complexes, therefore, maintaining the membrane skeleton in a taut state.

Actin-Filament Connection to the Membrane Skeleton

Actin is the major protein of the resting cytoskeleton. Actin filaments bind to the cytoplasmic side of spread membrane skeletons by both their sides and ends. The biochemical and histochemical data indicate that both spectrin and ABP molecules could mediate this linkage. Since the affinity of ABP for actin and of ABP for GPIb/IX are relatively high, and since GPIb/IX are transmembrane proteins, the coherence of the resting platelet cytoskeleton, alluded to above, could be assured. Whether platelet spectrin tetramers interconnect only on the ends of these long actin filaments or also through short actin oligomers as in the erythrocyte, remains to be determined. Our morphological observations indicate that at least some of the spectrin strands are directly connected with actin filaments (Fig. 6) and it is interesting that we estimate that there are four spectrin tetramers for every actin filament end in the platelet cytoskeleton. It is possible that platelet spectrin tetramers, however, could attach multiple times to actin filaments running parallel to the plasma membrane, although we would have expected to find such actin filaments remaining attached to the total membrane skeleton if this was the predominant interaction.

We thank Dr. Thomas P. Stossel for his supportive environment, wonderful ideas, and helpful criticism and Ms. Darlene Jackson for her editorial and secretarial skills. We also are grateful to Dr. Peter Walley of Cressington for designing a useful, reliable Freeze-Fracture Machine and for his help in evaporating tantalum-tungsten metals.

Supported by U.S. Public Health Service grants HL-19429 and GM-36507 and by grants from the Council for Tobacco Research USA and the Edwin S. Webster Foundation.

Received for publication 23 February 1990 and in revised form 29 October 1990.

References

1. Boyles, J., J. E. B. Fox, D. R. Phillips, and P. E. Stenberg. 1985. Organization of the cytoskeleton in resting, discoid platelets: preservation of actin filaments by a modified fixation that prevents osmium damage. *J. Cell Biol.* 101:1463–1472.
2. Ezzell, R., D. Kenney, S. Egan, T. Stossel, and J. Hartwig. 1988. Localization of the domain of actin-binding protein that binds to membrane glycoprotein Ib and actin in human platelets. *J. Biol. Chem.* 263:13303–13309.
3. Fox, J. 1985. Identification of actin-binding protein as the protein linking the membrane skeleton to glycoproteins on platelet plasma membrane. *J. Biol. Chem.* 260:11970–11977.
4. Fox, J., L. Aggerbeck, and M. Berndt. 1988. Structure of the glycoprotein Ib-IX complex from platelet membranes. *J. Biol. Chem.* 263:4882–4890.
5. Fox, J., J. Boyles, M. Berndt, P. Steffen, and L. Anderson. 1988. Identification of a membrane skeleton in platelets. *J. Cell Biol.* 106:1525–1538.
6. Fox, J., C. Reynolds, J. Morrow, and D. Phillips. 1987. Spectrin is associated with membrane-bound actin filaments in platelets and is hydrolyzed by the Ca^{2+}-dependent protease during platelet activation. *Blood.* 69:537–545.
7. George, J., E. Pickett, S. Saucerman, R. McEver, T. Kunicki, N. Kieffer, and P. Newman. 1986. Platelet surface glycoproteins. *J. Clin. Invest.* 78:340–348.
8. Glenney, J., P. Glenney, and K. Weber. 1982. Erythroid spectrin, brain fodrin, and intestinal brush border proteins (TW-260/240) are related molecules containing a common calmodulin-binding subunit bound to a variant cell type-specific subunit. *Proc. Natl. Acad. Sci. USA.* 79:4002–4005.
9. Hartwig, J., and P. Shevlin. 1986. The architecture of actin filaments and the ultrastructural location of actin-binding protein in the periphery of lung macrophages. *J. Cell Biol.* 103:1007–1020.
10. Hartwig, J., K. Chambers, K. Hopcia, and D. Kwiatkowski. 1989. Association of profilin with filament-free regions of human leukocyte and platelet membranes and reversible membrane-binding during platelet activation. *J. Cell Biol.* 109:1571–1579.
11. Hartwig, J., K. Chambers, and T. Stossel. 1989. Association of gelsolin with actin filaments and cell membranes of macrophages and platelets. *J. Cell Biol.* 109:467–479.
12. Laemmli, U. 1970. Cleavage of structural proteins during the assembly of the head of bacteriophage T4. *Nature (Lond.).* 227:680–685.
13. Lassing, I., and U. Lindberg. 1988. Evidence that the phosphatidylinositol cycle is linked to cell motility. *Exp. Cell Res.* 174:1–15.
14. Lind, S. E., P. A. Janmey, C. Chaponnier, T. Herbert, and T. P. Stossel. 1987. Reversible binding of actin to gelsolin and profilin in human platelet extracts. *J. Cell Biol.* 105:833–842.
15. Liu, S.-C., L. Derick, and J. Palek. 1987. Visualization of the hexagonal lattice in the erythrocyte membrane skeleton. *J. Cell Biol.* 104:527–536.
16. Loftus, J., J. Choate, and R. Albrecht. 1984. Platelet activation and cytoskeletal reorganization: high voltage electron microscopic examination of intact and triton-extracted whole mounts. *J. Cell Biol.* 98: 2019–2025.
17. McGough, A., and R. Josephs. 1990. On the structure of erythrocyte spectrin in partially expanded membrane skeletons. *Proc. Natl. Acad. Sci. USA.* 87:5208–5212.
18. Michelson, A., and M. Barnard. 1987. Thrombin-induced changes in platelet membrane glycoproteins Ib, IX, and IIb-IIIa complex. *Blood.* 70:1673–1678.
19. Morrow, J. 1989. The spectrin membrane skeleton: emerging concepts. *Curr. Op. Cell Biol.* 1:23–29.
20. Nachmias, V. 1980. Cytoskeleton of human platelets at rest and after

spreading. *J. Cell Biol.* 86:795–802.
21. Nachmias, V., J. Sullender, J. Fallon, and A. Asch. 1979. Observations on the "cytoskeleton" of human platelets. *Thromb. Haemostasis. (Stuttg.)* 42:1661–1666.
22. Nachmias, V. T., and K. Yoshida. 1988. The cytoskeleton of the blood platelet: a dynamic structure. *Adv. Cell Biol.* 2:181–211.
23. Nakata, T., and N. Hirokawa. 1987. Cytoskeletal reorganization in human platelets after stimulation revealed by the quick-freeze deep-etch technique. *J. Cell Biol.* 105:1771–1780.
24. O'Halloran, T., M. C. Beckerle, and K. Burridge. 1985. Identification of talin as a major cytoplasmic protein implicated in platelet activation. *Nature (Lond.).* 317:449–451.
25. Okita, L., D. Pidard, P. Newman, R. Montogomery, and T. Kunicki. 1985. On the association of glycoprotein Ib and actin-binding protein in human platelets. *J. Cell Biol.* 100:317–321.
26. Pinder, J. C., A. G. Weeds, and W. B. Gratzer. 1986. Study of actin filament ends in the human red cell membrane. *J. Mol. Biol.* 191:461–468.
27. Pollard, T., K. Fujiwara, R. Handin, and G. Weiss. 1977. Contractile proteins in platelet activation and contraction. *Ann. NY Acad Sci.* 283: 218–236.
28. Rosenberg, S., A. Stracher, and R. Lucas. 1981. Isolation and characterization of actin and actin-binding protein from human platelets. *J. Cell Biol.* 91:201–211.
29. Safer, D., R. Golla, and V. Nachmais. 1990. Isolation of a 5-kilodalton actin-sequestering peptide from human blood platelets. *Proc. Natl. Acad. Sci. USA.* 87:2536–2540.
30. Schliwa, M., J. van Blerkom, and K. Porter. 1981. Stabilization of the cytoplasmic ground substance in detergent-opened cells and a structural and biochemical analysis of its composition. *Proc. Natl. Acad. Sci. USA.* 80:5417–5420.
31. Schollmeyer, J., G. Rao, and J. White. 1978. An actin-binding protein in human platelets. *Am. J. Pathol.* 93:433–445.
32. Shen, B. W., R. Josephs, and T. L. Steck. 1986. Ultrastructure of the intact skeleton of the human erythrocyte membrane. *J. Cell Biol.* 102:997–1006.
33. Sixma, J., A. van den Berg, B. Jockusch, and J. Hartwig. 1989. Immunoelectron microscopic localization of actin, α-actinin, actin-binding protein and myosin in resting and activated human blood platelets. *Eur. J. Cell Biol.* 48:271–281.
34. Slot, J., and H. Geuze. 1985. A new method of preparing gold probes for multiple-labeling cytochemistry. *Eur. J. Cell Biol.* 38:87–93.
35. Stendahl, O., J. Hartwig, E. Brotschi, and T. Stossel. 1980. Distribution of actin-binding protein and myosin in macrophages during spreading and phagocytosis. *J. Cell Biol.* 84:215–224.
36. Stossel, T. 1989. From signal to pseudopod. How cells control cytoplasmic actin assembly. *J. Biol. Chem.* 264:18261–18264.
37. Takeuchi, K., K. Kuroda, M. Ishigami, and T. Nakamura. 1990. Actin cytoskeleton of resting bovine platelets. *Exp. Cell Res.* 186:374–380.
38. Towbin, J., T. Staehelin, and J. Gordon. 1979. Electrophoretic transfer of proteins from polyacrylamide gels to nitrocellulose sheets: procedure and some applications. *Proc. Natl. Acad. Sci. USA.* 76:4350–4354.
39. Tyler, J. M., J. M. Anderson, and D. Branton. 1980. Structural comparison of several actin-binding molecules. *J. Cell Biol.* 85:489–495.
40. White, J. 1984. Arrangements of actin filaments in the cytoskeleton of human platelets. *Am. J. Pathol.* 117:207–217.
41. Yin, H. L., D. J. Kwiatkowski, J. E. Mole, and F. S. Cole. 1984. Structure and biosynthesis of cytoplasmic and secreted variants of gelsolin. *J. Biol. Chem.* 259:5271–5276.